

UNIVERSIDADE ESTADUAL DE CAMPINAS
SISTEMA DE BIBLIOTECAS DA UNICAMP
REPOSITÓRIO DA PRODUÇÃO CIENTÍFICA E INTELLECTUAL DA UNICAMP

Versão do arquivo anexado / Version of attached file:

Versão do Editor / Published Version

Mais informações no site da editora / Further information on publisher's website:

<https://aip.scitation.org/doi/10.1063/1.4942613>

DOI: 10.1063/1.4942613

Direitos autorais / Publisher's copyright statement:

©2016 by AIP Publishing. All rights reserved.

DIRETORIA DE TRATAMENTO DA INFORMAÇÃO

Cidade Universitária Zeferino Vaz Barão Geraldo

CEP 13083-970 – Campinas SP

Fone: (19) 3521-6493

<http://www.repositorio.unicamp.br>

Impact of the intermixed phase and the channel network on the carrier mobility of nanostructured solar cells

Cristiano F. Woellner¹ and José A. Freire^{2,a)}

¹*Department of Applied Physics, University of Campinas, Campinas, SP 13083-970, Brazil*

²*Departamento de Física, Universidade Federal do Paraná, Curitiba, PR 81531-990, Brazil*

(Received 22 December 2015; accepted 10 February 2016; published online 29 February 2016)

We analyzed the impact of the complex channel network of donor and acceptor domains in nanostructured solar cells on the mobility of the charge carriers moving by thermally activated hopping. Particular attention was given to the so called intermixed phase, or interface roughness, that has recently been shown to promote an increase in the cell efficiency. The domains were obtained from a Monte Carlo simulation of a two-species lattice gas. We generated domain morphologies with controllable channel size and interface roughness. The field and density dependence of the carrier hopping mobility in different morphologies was obtained by solving a master equation. Our results show that the mobility decreases with roughness and increases with typical channel sizes. The deleterious effect of the roughness on the mobility is quite dramatic at low carrier densities and high fields. The complex channel network is shown to be directly responsible for two potentially harmful effects to the cell performance: a remarkable decrease of the mobility with increasing field and the accumulation of charge at the domains interface, which leads to recombination losses. © 2016 AIP Publishing LLC. [<http://dx.doi.org/10.1063/1.4942613>]

I. INTRODUCTION

In bulk heterojunction (BHJ) solar cells,^{1,2} an electron donor, typically a conjugated polymer³ or a small-molecule,^{4,5} and an electron acceptor molecule are mixed so as to form a nanoscale phase separated structure. Traditionally the donor polymer is some variant of poly(3-hexylthiophene-2,5-diyl), P3HT,⁶ and the acceptor molecule is some variant of a fullerene.⁷ The photon is mostly absorbed in the polymer and the resulting exciton diffuses to the interface where it dissociates.⁸ Following dissociation, the electron and the hole move by thermally activated hopping through the acceptor and donor domains, respectively.

In conjugated polymer-based BHJ solar cells, the polymer and the fullerene are deposited in solution. As the mixture solidifies, some polymers tend to form crystallites^{9–12} that expel the fullerene molecule towards the amorphous polymeric region wherein some aggregates of fullerene molecules can be found. This complex morphology contains intertwined pure-donor and pure-acceptor domains, together with intermixed domains. Transmission electron microscopy suggests domain sizes of the order of 10–30 nm.¹³ For a review on the morphology of BHJ solar cells see Refs. 14 and 15. For evidences on the existence of the intermixed phase see Refs. 16–20.

Recently the intermixed phase has been associated with an increase in the cell power conversion efficiency.^{20,21} This increase has been linked to an increase in charge photo-generation.²² There is also evidence of the importance of pure domains to achieve high cell performance.²³

The size of the pure domains should affect the cell performance in two opposing ways. On the one hand, smaller domains reduce the distance that the exciton has to diffuse to reach the nearest interface, which enhances photo-charge generation and cell efficiency, but on the other hand, smaller domain sizes make the percolating path of the photo-generated charge more winding, which likely reduces the effective carrier mobility and cell efficiency.

The intermixed phase should also affect the cell performance in two opposing ways. On the one hand, intermixed domains enhance exciton dissociation,²² which improves cell performance, but on the other hand, the charge mobility through the intermixed phase must be very low, which contributes to reduce the cell efficiency.¹³

Our goal is to investigate how the pure domains size and the intermixed phase affect the carrier mobility. We will only consider the effect of the channel morphology on the carrier mobility. Charge generation/recombination, as well as Coulomb interaction, will not enter explicitly in the model. In the Conclusion, we explain how to link our result with these two physical effects.

We employ a lattice hopping model of a two-phase system already used in a previous publication.²⁴ The domain morphology was generated using a Monte-Carlo simulation of a two-species lattice gas that allowed us to generate morphologies with different degrees of phase separation and interface roughness. The interface roughness plays the role of the intermixed phase between pure domains.

The carrier mobilities were calculated assuming thermally activated transport and using a master equation, see Refs. 24–26 for examples of this type of calculation. The field and density dependence of the charge mobility was analyzed for different domain morphologies.

^{a)}jfreire@fisica.ufpr.br

II. MODEL

A. Morphology production

We employed a two species lattice gas model where each site either contains a species A or B (no vacancies were allowed). The sites intend to represent the transport units of the donor and the acceptor that the electrons and holes use to move about the cell via thermally activated hopping, but their identification with the fullerene and the conjugation length of the P3HT present some problems since, while the fullerene crystal lattice spacing is well defined (~ 1 nm²⁷), the typical conjugation length of P3HT varies greatly depending on the processing conditions. Instead of viewing our model as a faithful representation of the actual BHJ cell, one should view it as the simplest model that contains intertwined and intermixed phases also present in the actual BHJ cell. Our aim is at understanding the effect of this type of morphology on the hopping mobility, rather than describing the effect.

Starting with a random configuration that filled a cubic lattice with A and B species in a 50% volume ratio, which guarantees a percolating network for both type of sites, a Monte Carlo simulation moved the A and B particles according to the change in the total energy of the configuration. This energy was obtained associating an energy ϵ_{AA} to two nearest neighbors A particles (similarly for ϵ_{BB} and ϵ_{AB}). Depending on the values of these three energies and on the point of the simulation we chose to stop, we were able to control the typical channel size of the pure domains and the level of interface roughness, our representation of the intermixed phase. Examples of some morphologies are shown in Fig. 1.

B. Morphology characterization

The parameter b used to characterize the channel size of the percolating domain was designed to be independent of the interface roughness. We decomposed the cubic volume in a set of $3N^2$ chains of N sites (N^2 chains per Cartesian direction). On each chain, we computed the average (straight-A or straight-B) segment size belonging to the percolating domain, ignoring single sites and assuming periodic boundary conditions. The parameter b is the average of this quantity over all $3N^2$ chains. This parameter captures the typical size of the channels in the percolating domain in units of the lattice parameter.

The parameter g used to characterize the interface roughness was the average of the total interfacial area of the percolating domain by the number of interfacial sites in the percolating domain. This parameter is therefore the average number of A-B interfaces per interfacial site. In a cubic lattice, this is a number between 1 (perfect smoothness) and 5 (maximum roughness). We were only able to obtain values between 1.3 and 2.1.

Since we used a 50% volume ratio, the A and B percolating domains are very similar and so are their b and g parameters, see Fig. 1. All systems considered had 50^3 sites ($N = 50$).

C. The mobility

The mobility was computed using a master equation for the site average occupation. Only nearest neighbor hopping was considered, periodic boundary conditions were used in

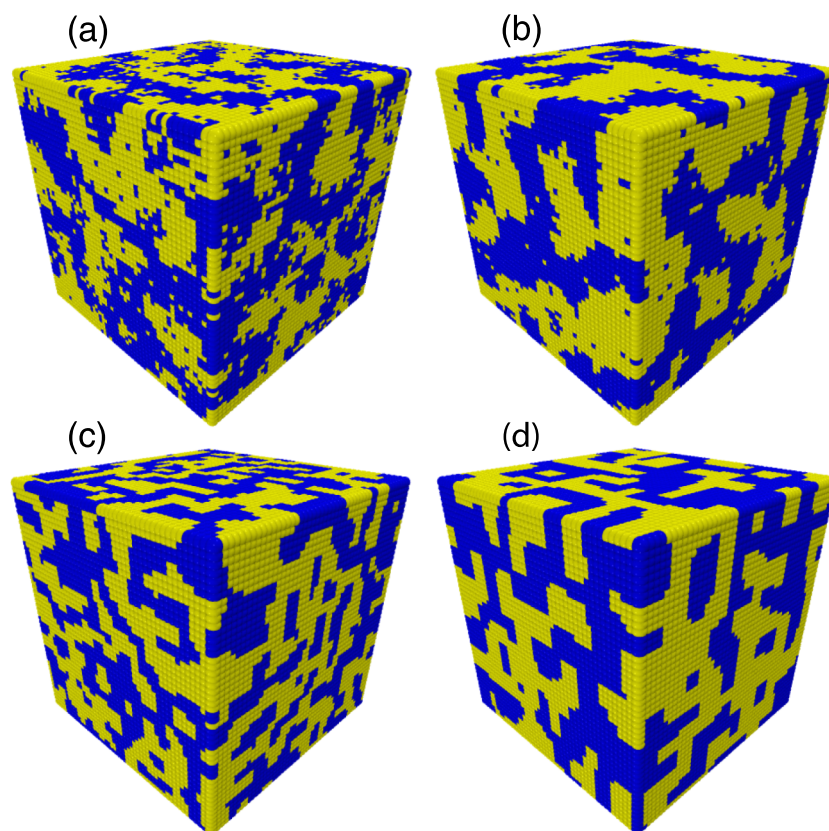


FIG. 1. Distribution of two species over a cubic lattice in a 50% volume ratio. Systems (a) and (b) have rough interfaces ($g \sim 1.9$); systems (c) and (d) have smooth interfaces ($g \sim 1.5$). Systems (a) and (c) have small channels ($b \sim 6.2$); systems (b) and (d) have large channels ($b \sim 9.1$). The values of b and g for both yellow and blue domains are similar.

all three Cartesian directions and site double occupancy was forbidden. The master equation reads

$$\frac{dP_n}{dt} = \sum_k [W_{k \rightarrow n} P_k (1 - P_n) - W_{n \rightarrow k} P_n (1 - P_k)], \quad (1)$$

where k is a nearest neighbor of n and P_k is the occupancy of site k . To this set of equations, we added an extra one fixing the average site occupancy,

$$n = \frac{1}{N^3} \sum_k P_k. \quad (2)$$

The energies of the A and B sites were taken as random variables whose mean was offset by 0.9 eV. This being an average of the energy offset of the LUMOs (~ 1.0 eV) and of the HOMOs (~ 0.8 eV) in P3HT and PCBM. The charge transport we shall describe can be either viewed as electron transport through the acceptor LUMOs or hole transport through the donor HOMOs. We did not model the process of charge generation nor the process of charge recombination.

The site energies also had a (Gaussian) dispersion of 0.1 eV about their mean to account for local environment disorder, a typical value in disordered organic systems.

The hopping rates between two given neighboring sites depend on the sites energies u , which in turn are affected by the internal electric field \mathbf{E} , and on the distance between sites (here assumed to be fixed and equal to the lattice parameter a). We used the Miller-Abrahams hopping rate.²⁸ For a carrier of charge q , it reads

$$W_{k \rightarrow n} = w_0 e^{-2\gamma a} \min\{1, e^{-(u_n - u_k)/k_B T}\}, \quad (3)$$

$$u_n = \epsilon_n - q\mathbf{E} \cdot \mathbf{r}_n, \quad (4)$$

where w_0 is an attempt frequency, γ is an inverse localization length, ϵ_n is the random site energy, \mathbf{r}_n is the position of site n , T is the temperature, and k_B is Boltzmann's constant. We used a lattice spacing $a = 1$ nm (typical distance between fullerenes²⁷), $\gamma = 10/a$,²⁵ $w_0 = 4.8 \times 10^{20} \text{ s}^{-1}$,²⁹ and $kT = 25$ meV (room temperature). These parameters lead to a maximum nearest neighbor hopping rate $\sim 10^{12} \text{ s}^{-1}$, in accord with the estimates of Ref. 30.

We used $a = 1$ nm in our calculations but this value may be inadequate to model the conjugated polymer. In fact, the determination the proper lattice parameter to model the hopping transport in a disordered organic material is a quite difficult problem.

From the steady-state solution of Eqs. (1) and (2), we obtained the average current density using

$$J = \frac{q}{a^2 N^2} \sum_{n,n'} [W_{n \rightarrow n'} P_n^s (1 - P_{n'}^s) - W_{n' \rightarrow n} P_{n'}^s (1 - P_n^s)], \quad (5)$$

where n and n' are nearest neighbor sites belonging to adjacent planes orthogonal to the field direction and a is the cubic lattice parameter. The mobility follows from $\mu = J/nqE$. The mobilities presented below were obtained from an average of the mobilities along the three Cartesian directions.

In Fig. 2, we show the zero-field mobility (for a very small carrier density) as a function of the typical channel size (b) and interface roughness (g) of the percolating domain. It is clear that the mobility is favored by large domains (large b)

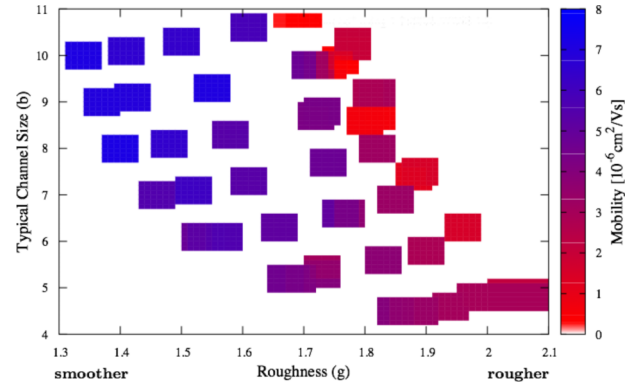


FIG. 2. Zero-field mobility as a function of the roughness parameter g and the characteristic channel size b , for very small carrier density. The mobility is favored by large channels and smoother interfaces.

and smooth interfaces (small g), as it was expected. However, the impact of the morphology on the zero-field mobility does not seem to be very dramatic (at most a factor of 10 for the morphologies considered).

We next investigated the field and carrier density dependence of the mobility of the four systems showed in Fig. 1, which are representative of extreme values of b and g . We recall that the field to be discussed in the following is an internal field. In a solar cell, small internal fields are present in the open circuit condition and large internal fields are present in the short circuit condition (in this case, the internal field is due to the difference in the electrodes work functions).

In Fig. 3, we show the mobility as a function of the internal field for (a) two systems with large channels, one with smooth and the other with rough interfaces and (b) two systems with small channels, one with smooth and the other with rough interfaces. The carrier densities considered were $8 \times 10^{15} \text{ cm}^{-3}$ and $8 \times 10^{18} \text{ cm}^{-3}$. The internal field values in Fig. 3 correspond to our choice of the lattice parameter, $a = 1$ nm. Since the internal field enters the master equation (Eq. (1)) in the form of the dimensionless parameter qEa/kT , an increase of the lattice parameter by a factor f would reduce the field values in Fig. 3 by $1/f$.

Both figures display an increase of the mobility with charge density, also seen in single species systems,²⁵ and an increase of the mobility with the smoothness of the interface. This last effect, which is very mild at zero-field, increases dramatically with the field, specially when the carrier density is low.

In comparing the mobilities of Figs. 3(a) and 3(b), we see that larger channels result in slightly larger mobilities. However, the impact of the channel size on the mobility is much weaker than that of the roughness.

The interface roughness in our model represents the intermixed phase in a real solar cell. Large roughness is expected to be accompanied by large carrier densities. Our result shows that the decrease in mobility due to roughness in systems with large carrier densities is not very dramatic. If the gain in carrier density caused by the intermixed phase is large enough, it may compensate for the decrease in mobility and result in an enhancement of the current density, $J \sim \mu n$.

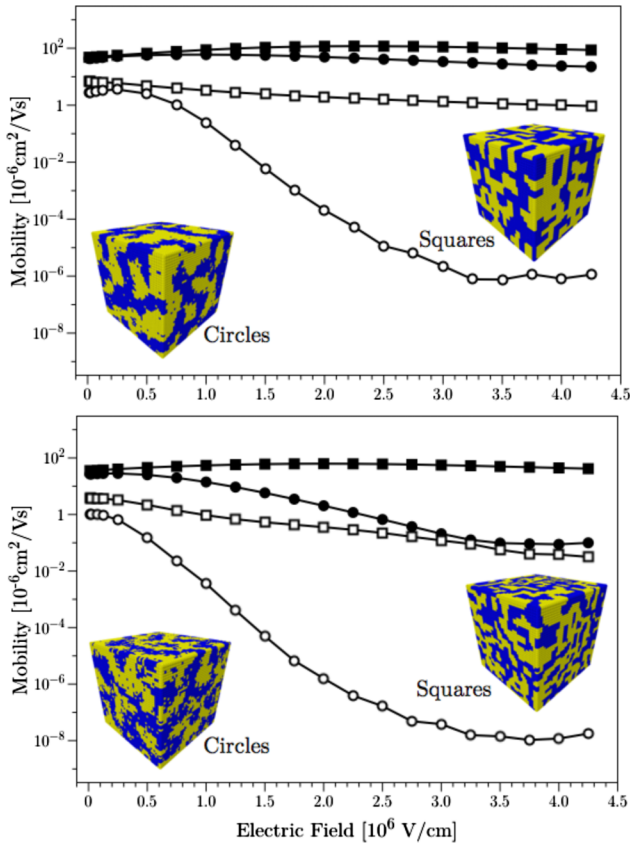


FIG. 3. Mobility as a function of the internal field: (a) two systems with large channels, one with rough interfaces (circles) and the other with smooth interfaces (squares) and (b) two systems with small channels, one with rough interfaces (circles) and the other with smooth interfaces (squares). The carrier densities considered were $n = 8 \times 10^{15} \text{ cm}^{-3}$ (open symbols) and $n = 8 \times 10^{18} \text{ cm}^{-3}$ (filled symbols).

In order to be more precise, we would have to include the exciton dissociation process in our model.

In Figs. 3(a) and 3(b), one also observes that some of the $\mu(E)$ curves show a decrease of the mobility with increasing field. This effect becomes more noticeable for low carrier densities and large interface roughness. This effect was observed experimentally in hopping transport in disordered organic systems³¹ and was associated with spatial disorder in the early days of the Gaussian Disorder Model (GDM).³² The point is that at small fields, there are some conduction paths that go against the field direction that contribute significantly to the total current only due to the spatial proximity of the sites (the spatial factor dominates over the energy factor in Eq. (3)). As the field increases, the change in the site energies end up making the energy factor in the rate dominant and the

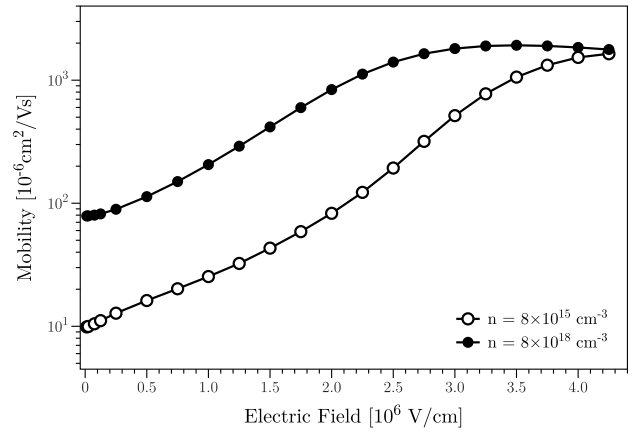


FIG. 4. Mobility as a function of the electric field for a single-phase system that used the same parameters of the four two-phase systems of Figs. 3(a) and 3(b). The mobility increases monotonically with the field.

total rate becomes very small. This type of conduction path is eliminated with increasing field and the mobility decreases.

In our system, we have no spatial disorder; the effect is due to the channel network. To prove this point, we show in Fig. 4 the field dependence of the mobility of a single-phase (homogeneous) system that used parameters identical to the ones used for the four two-phase systems in Figs. 3(a) and 3(b). No decay of μ with the field is observed.

To visualize the effect of the field on the major current paths, we must first identify the sites that belong to the major current paths. Any given site is linked by six bonds to its neighbors. Each bond is associated to a net current that may be inbound to or outbound from the given site (the total inbound current equals the total outbound current at any given site in the steady state). We identified the sites belonging to a major current path by the magnitude of the total inbound current to that site. The point is illustrated in two dimensions in Fig. 5.

The upper panels of Fig. 6 highlight those sites whose current going through them was larger than a fraction $1/N^2$ of the total current. The left panel corresponds to a small field ($0.05 \times 10^6 \text{ V/cm}$) and the right panel to a large field ($2.5 \times 10^6 \text{ V/cm}$). The field is in the horizontal direction and drives the charges to the left. It is clear that certain channels perpendicular to the field direction cease to contribute to the total current with increasing field. As the field increases, the current paths become more aligned with the field, occupying whatever channels along the field direction they can find. In a complex channel network morphology, many current paths



FIG. 5. Two sites and the net currents along the four bonds to their neighbors (not shown). The total inbound current (sum of the red arrows lengths) and the total outbound current (sum of the green arrows lengths) are equal in both cases, but there is a larger current going through the left site than through the right site.

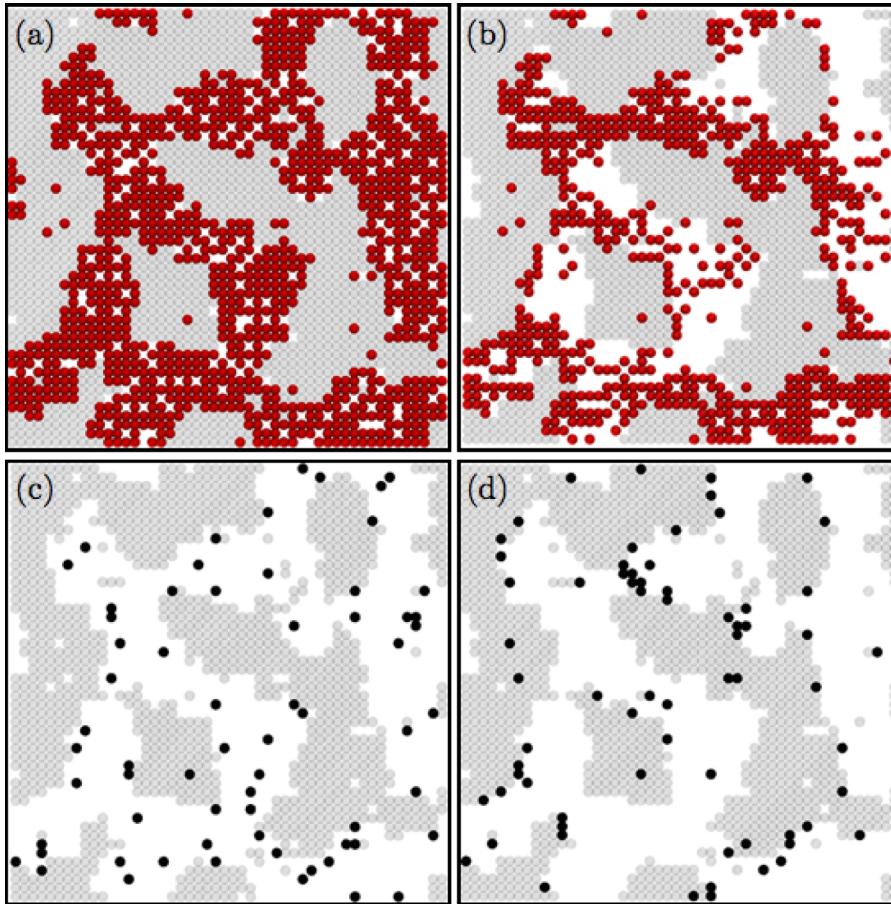


FIG. 6. A given plane along the field direction of the system corresponding to the open circles in Fig. 3(a). The charges are driven by the field to move to the left along the white domain. In the upper panels, we highlight in red those sites whose current going through them was larger than a fraction $1/N^2$ of the total current, in the lower panels we highlight in black the sites that contain a significant fraction of the total amount of charge. The left panels correspond to a small field (0.05×10^6 V/cm) and the right panels to a large field (2.5×10^6 V/cm).

cease to contribute to the total current as the field increases thus resulting in a decrease of the mobility.

This is not the only potentially harmful effect of the complex channel network to the cell performance. The lower panels of Fig. 6 highlight, for the same system and fields of the upper panels, the sites whose occupation corresponds to a significant fraction of the total amount of carriers. It is evident that at large fields, there is a significant concentration of charge at the interfaces between the two phases. In an actual cell, these sites would act as recombination centers that would lower the cell performance.

Both effects illustrated in Fig. 6 can only be avoided if the domain channels are aligned with the field direction.

III. SUMMARY AND CONCLUSIONS

We examined the effect of the interface roughness and channel network of a two-phase system on the carrier hopping mobility. The interface roughness aimed at modeling the intermixed phase of a BHJ solar cell. Our results suggests that (i) the effect of the intermixed phase on the zero-field mobility is very mild, Fig. 2; (ii) but its effect on the mobility field dependence can be quite dramatic, Figs. 3(a) and 3(b), reaching a factor of up to six orders of magnitude for low carrier densities and at high fields; (iii) the domain channel network results in a decrease of the mobility with increasing field, an effect that is seen in single-phase systems only when positional disorder is present.³² This effect is greatly enhanced by the intermixed phase when the carrier density is

low and is due to channels perpendicular to the field direction ceasing to contribute to the total current with increasing field, Figs. 6(a) and 6(b); (iv) at large fields, the carrier accumulates at interfacial sites, Figs. 6(c) and 6(d), which may end-up acting as recombination centers.

Large internal fields are present in a solar cell in the short current condition. The decrease of the mobility with the field caused by the channel network and the roughness would impact J_{sc} ; however, we showed that the effect is weakened by the presence of a large carrier density. Since large interface roughness, i.e., the presence of an intermixed phase, leads to an increase in the carrier density in an actual cell,²² it may happen that the intermixed phase results in an increase of $J_{sc} \sim n\mu$. We cannot be more precise since we did not model the effect of the channel morphology on the charge generation and recombination.

The field and density dependent mobility here discussed ignored charge generation and recombination, as well as Coulomb interaction. The simplest way to incorporate these effects is through a continuous model for the cell containing: (i) electron and hole continuity equations, with generation and recombination terms and expressions for $\mu(n, E)$ as suggested by our work; (ii) a Poisson equation relating the local field to the electron and hole densities.

The effect of the channel morphology on the field dependence of the mobility, see Fig. 3, could also, in principle, be directly observed in a time-of-flight experiment on an actual BHJ cell. To our knowledge, this has not yet been attempted.

It is worth mentioning that the decrease of the mobility with the internal field may, or may not, be observed in the operating regime of an actual cell, all depends on the appropriate value of lattice spacing to be used to model the cell materials, see discussion in Sec. II.

The concentration of charge at interfacial sites at large fields, Figs. 6(c) and 6(d), represents another mechanism of current degradation, this interfacial sites would act as electron/hole traps and/or electron-hole recombination centers.³³ Again, to be quantitative, we would have to model the recombination process in the dynamics.

Both effects, the decrease of the mobility with increasing fields and the accumulation of charge at the domain interfaces leading to recombination losses, are an inescapable consequence of the complex channel network. These deleterious effects would be suppressed only if the channels were aligned to the field direction.

Our model of transport is admittedly quite simplistic, particularly on its description of the polymer. Recently the role of tie polymers on the hopping transport in conjugated polymers has been stressed, see, for instance, Ref. 12. However, our aim was to understand the general effects of the morphology of a two-phase system on the charge mobility and we believe that the effects here addressed would also be present in a more realistic model of the BHJ solar cell.

The importance of our work rests on (i) its originality; (ii) the possibility of using our insight about $\mu(n, E)$ in a continuous model for the cell (that should include a continuity equation containing carrier generation/recombination and a Poisson equation); (iii) the possibility (in principle) of directly measuring the $\mu(n, E)$ of the BHJ cell, for instance, in a time-of-flight experiment³⁰ in the dark.

ACKNOWLEDGMENTS

C.F.W. thanks D. Galvão, P. Autreto, and L. Machado for their useful comments and suggestions. C.F.W. thanks CNPq and São Paulo Research Foundation (FAPESP) Grant No. 2014/24547-1 for financial support. Computational and financial support from the Center for Computational Engineering and Sciences at Unicamp through the FAPESP/CEPID Grant No. 2013/08293-7 is acknowledged.

¹G. Yu, J. Gao, J. C. Hummelen, F. Wudl, and A. J. Heeger, *Science* **270**, 1789 (1995).

²S. H. Park, A. Roy, S. Beaupre, S. Cho, N. Coates, J. S. Moon, D. Moses, M. Leclerc, K. Lee, and A. J. Heeger, *Nat. Photonics* **3**, 297 (2009).

³S. Günes, H. Neugebauer, and N. S. Sariciftci, *Chem. Rev.* **107**, 1324 (2007).

⁴M. Riede, T. Mueller, W. Tress, R. Schueppel, and K. Leo, *Nanotechnology* **19**, 424001 (2008).

⁵Y. Sun, G. C. Welch, W. L. Leong, C. J. Takacs, G. C. Bazan, and A. J. Heeger, *Nat. Mater.* **11**, 44 (2012).

⁶W. Ma, C. Yang, X. Gong, K. Lee, and A. J. Heeger, *Adv. Funct. Mater.* **15**, 1617 (2005).

⁷A. Zusan, K. Vandewal, B. Allendorf, N. H. Hansen, J. Pflaum, A. Salleo, V. Dyakonov, and C. Deibel, *Adv. Energy Mater.* **4**, 1400922 (2014).

⁸O. V. Mikhnenko, P. W. M. Blom, and T.-Q. Nguyen, *Energy Environ. Sci.* **8**, 1867 (2015).

⁹A. Zen, M. Saphiannikova, and D. Neher, *Macromolecules* **39**, 2162 (2006).

¹⁰Y. Kim, S. Cook, S. M. Tuladhar, S. A. Choulis, J. Nelson, J. R. Durrant, D. D. C. Bradley, M. Giles, I. McCulloch, C.-S. Ha, and M. Ree, *Nat. Mater.* **5**, 197 (2006).

¹¹C. J. Takacs, N. D. Treat, S. Krämer, Z. Chen, A. Facchetti, M. L. Chabinyc, and A. J. Heeger, *Nano Lett.* **13**, 2522 (2013).

¹²R. Noriega, J. Rivnay, K. Vandewal, F. P. V. Koch, N. Stingelin, P. Smith, M. F. Toney, and A. Salleo, *Nat. Mater.* **12**, 1038 (2013).

¹³X. Yang, J. Loos, S. C. Veenstra, W. J. H. Verhees, M. M. Wienk, J. M. Kroon, M. A. J. Michels, and R. A. J. Janssen, *Nano Lett.* **5**, 579 (2005).

¹⁴P. W. M. Blom, V. D. Mihailescu, L. J. A. Koster, and D. E. Markov, *Adv. Mater.* **19**, 1551 (2007).

¹⁵N. D. Treat and M. L. Chabinyc, *Annu. Rev. Phys. Chem.* **65**, 59 (2014).

¹⁶B. Watts, W. J. Belcher, L. Thomsen, H. Ade, and P. C. Dastoor, *Macromolecules* **42**, 8392 (2009).

¹⁷B. A. Collins, E. Gann, L. Guignard, X. He, C. R. McNeill, and H. Ade, *J. Phys. Chem. Lett.* **1**, 3160 (2010).

¹⁸M. Pfannmöller, H. Flügge, G. Benner, I. Wacker, C. Sommer, M. Hanselmann, S. Schmale, H. Schmidt, F. A. Hamprecht, T. Rabe, W. Kowalsky, and R. R. Schröder, *Nano Lett.* **11**, 3099 (2011).

¹⁹N. D. Treat, M. A. Brady, G. Smith, M. F. Toney, E. J. Kramer, C. J. Hawker, and M. L. Chabinyc, *Adv. Energy Mater.* **1**, 82 (2011).

²⁰N. D. Treat, A. Varotto, C. J. Takacs, M. Al-Hashimi, J. Martin, A. J. Heeger, F. Wudl, C. J. Hawker, and M. L. Chabinyc, *J. Am. Chem. Soc.* **134**, 15869 (2012).

²¹P. A. Troshin, H. Hoppe, J. Renz, M. Egginger, J. Y. Mayorova, A. E. Goryachev, A. S. Peregodov, R. N. Lyubovskaya, G. Gobsch, N. S. Sariciftci, and V. F. Razumov, *Adv. Funct. Mater.* **19**, 779 (2009).

²²P. Westacott, J. R. Tumbleston, S. Shoaee, S. Fearn, J. H. Bannock, J. B. Gilchrist, S. Heutz, J. DeMello, M. Heeney, H. Ade, J. R. Durrant, D. S. McPhail, and N. Stingelin, *Energy Environ. Sci.* **6**, 2756 (2013).

²³S. Shoaee, S. Subramanian, H. Xin, C. Keiderling, P. S. Tuladhar, F. Jamieson, S. A. Jenekhe, and J. R. Durrant, *Adv. Funct. Mater.* **23**, 3286 (2013).

²⁴C. F. Woellner, Z. Li, J. A. Freire, G. Lu, and T.-Q. Nguyen, *Phys. Rev. B* **88**, 125311 (2013).

²⁵W. F. Pasveer, J. Cottaar, C. Tanase, R. Coehoorn, P. A. Bobbert, P. W. M. Blom, D. M. de Leeuw, and M. A. J. Michels, *Phys. Rev. Lett.* **94**, 206601 (2005).

²⁶L. J. A. Koster, *Phys. Rev. B* **81**, 205318 (2010).

²⁷M. Casalegno, S. Zanardi, F. Frigerio, R. Po, C. Carbonera, G. Marra, T. Nicolini, G. Raos, and S. V. Meille, *Chem. Commun.* **49**, 4525 (2013).

²⁸A. Miller and E. Abrahams, *Phys. Rev.* **120**, 745 (1960).

²⁹J.-L. Brédas, D. Beljonne, V. Coropceanu, and J. Cornil, *Chem. Rev.* **104**, 4971 (2004).

³⁰H. Bässler, *Phys. Status Solidi B* **107**, 9 (1981).

³¹P. M. Borsenberger, L. Pautmeier, and H. Bässler, *J. Chem. Phys.* **94**, 5447 (1991).

³²H. Bässler, *Phys. Status Solidi B* **175**, 15 (1993).

³³S. R. Cowan, A. Roy, and A. J. Heeger, *Phys. Rev. B* **82**, 245207 (2010).